

A bulk mass flux convection scheme for climate model: description and moisture sensitivity

Daehyun Kim · In-Sik Kang

Received: 19 July 2010 / Accepted: 18 December 2010 / Published online: 4 January 2011
© Springer-Verlag 2011

Abstract A convection scheme for climate model is developed based on Tiedtke's (Mon Weather Rev 117:1779–1800, 1989) bulk mass flux framework and is evaluated with observational data and cloud resolving model simulation data. The main differences between the present parameterization and Tiedtke's parameterization are the convection trigger, fractional entrainment and detrainment rate formulations, and closure method. Convection is triggered if the vertical velocity of a rising parcel is positive at the level at which the parcel is saturated. The fractional entrainment rate depends on the vertical velocity and buoyancy of the parcel as well as the environmental relative humidity. For the fractional detrainment rate, a linear decrease in the updraft mass flux above maximum buoyancy level is assumed. In the closure method, the cloud base mass flux is determined by considering both cloud layer instability and subcloud layer turbulent kinetic energy as controlling factors in the strength of the convection. The convection scheme is examined in a single column framework as well as using a general circulation model. The present bulk mass flux (BMF) scheme is compared with a simplified Relaxed Arakawa-Schubert (RAS) scheme. In contrast to the RAS, which specifies the cloud top, cloud top height in BMF depends on environmental properties, by considering the

conditions of both the parcel and its environment in a fractional entrainment and detrainment rate formulations. As a result, BMF shows improved sensitivity in depth and strength of convection on environmental humidity compared to RAS, by strengthening coupling between cloud and environment. When the mid to lower troposphere is dry, the cloud resolving model and BMF produce cloud top around the dry layer and moisten the layer. In the framework of general circulation model, enhanced coupling between convection and environmental humidity in BMF results in improved representation of eastward propagating intraseasonal variability in the tropics—the Madden-Julian oscillation.

Keywords Cumulus parameterization · Moisture sensitivity · General circulation model

1 Introduction

1.1 Moisture sensitivity of convection

Moist convection is one of the most important phenomena in the atmosphere, considering its role of the redistribution of heat, moisture and momentum. It has been shown that the climate simulated by the general circulation model (GCM) heavily depends on the cumulus parameterization of the model. Representations of the diurnal cycle (Lee et al. 2008), convectively coupled equatorial waves (CCEWs, Lin et al. 2008) including the Madden-Julian Oscillation (MJO, Wang and Schlesinger 1999; Maloney and Hartmann 2001; Lee et al. 2003), the El Niño southern oscillation (ENSO, Wu et al. 2007; Kim et al. 2008; Neale et al. 2008) and the intertropical convergence zone (ITCZ, Wu et al. 2003) are significantly altered by changing cumulus parameterization and its detailed implementation.

D. Kim · I.-S. Kang (✉)
School of Earth and Environmental Sciences,
Seoul National University, Seoul 151-747, South Korea
e-mail: kang@climate.snu.ac.kr

D. Kim
e-mail: dkim@ldeo.columbia.edu

Present Address:

D. Kim
Lamont-Doherty Earth Observatory of Columbia University,
Palisades, NY 10964-1000, USA

Therefore, accurate representation of cumulus convection in the GCM is necessary for reliable simulations of the climate. Furthermore, the poor simulation of the above phenomena in contemporary GCMs (e.g. MJO—Lin et al. 2006) points to deficiencies in cumulus parameterization and the need for its additional development.

Several observational (Brown and Zhang 1997; Sherwood 1999; Bretherton et al. 2004; Sherwood et al. 2004; Takayabu et al. 2006; Holloway and Neelin 2009) studies emphasize the role of low-level tropospheric humidity as a regulator of cumulus convection in tropical oceanic regions. It is shown in the above studies that there is a statistically significant relationship between low-level tropospheric moisture and convection over various time scales ranging from 3-hourly to monthly. On the issue of causality, it is thought that a dry lower troposphere inhibits deep convection. This argument is supported by the results of a simple parcel model (Brown and Zhang 1997; Holloway and Neelin 2009), which show that an updraft parcel easily loses its buoyancy through entrainment in dry conditions.

Cloud resolving model (CRM) simulations in various configurations (Tompkins 2001; Grabowski 2003; Chaboureau et al. 2004; Derbyshire et al. 2004; Kuang and Bretherton 2006) support the simple parcel model results. A dry free troposphere inhibits the organization of deep convection in CRM simulations of the above modeling studies. Derbyshire et al. (2004) show that, with an idealized configuration, two different CRMs simulate deep and strong convection in wet conditions while a shallow and weak updraft is simulated in dry conditions. It seems that the sensitivity to free tropospheric moisture is one of the robust relationships between convection and the environment and therefore needs to be simulated in any convection schemes.

Unfortunately, the relationship between free tropospheric moisture and convection is hardly simulated with convective parameterization of climate models (Ridout 2002; Derbyshire et al. 2004; Biasutti et al. 2006). Derbyshire et al. (2004) compared single column models (SCMs) with cloud resolving models, focusing on the relationship. They showed that most of the SCMs lack the sensitivity of moist convection, characterized by cloud top height and the strength of the upward mass flux, on environmental humidity compared to CRMs. In other words, current convection schemes exhibit a poor ability to simulate proper sensitivity on environmental moisture. From the above observational, numerical simulation studies, we can conclude: (i) that cumulus convection has a robust relationship with environmental moisture, and (ii) that current convection schemes poorly represent the sensitivity of cloud top height and the strength of convection to environmental moisture. Here our aim is to improve the sensitivities in the bulk mass flux convection scheme framework.

1.2 Parameterization of entrainment rate

In the bulk mass flux convection scheme (Tiedtke 1989), one of the popular type of convection schemes used in many global and regional models, the fractional entrainment rate is related to cloud top because a large (small) degree of mixing results in a low (high) cloud top height. Therefore, the value of entrainment rate for deep convection is smaller than that of shallow convection when the same scheme is separately used to simulate both kinds of convection (Tiedtke 1989). To represent various cumulus clouds using one method, it seems necessary to have state-dependent entrainment which is small (large) when the environment is favorable for deep (shallow) convection. This is consistent with cloud resolving model results in that the entrainment rate is a function of both parcel and environment properties (Lin 1999).

The results of simple parcel models (Brown and Zhang 1997; Holloway and Neelin 2009) suggest that representation of the entrainment process, through which cumulus clouds are affected by the environment, is at the center of the problem. It is, unfortunately, hard to obtain entrainment rates from observation data because it needs information of in-cloud properties at very high spatial and temporal resolution. Instead, we can obtain that physical quantity from the numerical simulation of convection with a sufficiently high resolution. Several cloud resolving model studies have explicitly calculated the entrainment rate (Lin 1999; Cohen 2000; Swann 2001) from their simulation results. They show that the fractional entrainment rate is not constant in height, as in some mass flux schemes, but large near the cloud base and top. Furthermore, Lin (1999) suggests that a fractional entrainment rate depends on the buoyancy of the parcel.

Meanwhile, using the cloud-mean vertical velocity equation, Gregory (2001) has suggested a parameterization of the entrainment rate that depends on parcel buoyancy and vertical velocity. The derivation of the entrainment rate is made from the kinematic view of cloud parcel in that some portion of the kinetic energy generated by positive parcel buoyancy should be transferred to the air entrained into clouds (Grant and Brown 1999). The vertical velocity of the environment is assumed to be zero; therefore entrained air needs kinetic energy to go upward with the cloud air. We adopted his method with modification on the value of the fraction of kinetic energy to be transferred to the entrained air.

A bulk mass flux convection scheme is developed in this study regarding the above considerations. Firstly, based on the framework of the bulk mass flux representation of convection (Tiedtke 1989), the entrainment rate formulation is revised. We have added the moisture factor to Gregory (2001)'s parameterization. Bechtold et al. (2008)

applied a simple entrainment rate formulation based on environmental moisture to the ECMWF model. Their results show that the entrainment rate has huge positive impacts on both climate simulations and predictions. And, to consider both cloud layer instability and subcloud turbulent kinetic energy as a driving forcing for cumulus convection, the hybrid closure method, which combines closures for deep and shallow convection scheme, is used.

The paper is organized as follows. The next section describes the bulk mass flux scheme in detail. In Sect. 3, the models and datasets used are described. Moisture sensitivity is tested in an idealized single time step experiment in Sect. 4. Results from a GCSS moistening period experiment using SCM and long-term integrations of GCM are presented in Sect. 5. The summary and conclusions are given in Sect. 6.

2 Description of the convection scheme

In this chapter, the bulk mass flux (hereafter, BMF) convection scheme developed in this study is described. The BMF convection scheme represents an ensemble of cumulus clouds using a single cloud model. The mass flux convection scheme consists of three parts; which are (a) cloud base properties and trigger, (b) cloud model, and (c) closure. We follow Tiedtke (1989) for the formulations of effects of the convection scheme on the environment. And we adopted downdraft and rain re-evaporation processes from Numaguti et al. (1995).

2.1 Cloud base properties and triggering

At first, the scheme decides whether cumulus convection will be activated or not. Without an appropriate triggering process, convection could occur too frequently over the tropics, which could prevent the host model from properly simulating large-scale organization of convection (e.g. CCEWs). For a mass flux-type convection scheme (e.g. Arakawa and Schubert 1974), triggering based on environmental humidity (Wang and Schlesinger 1999) and boundary layer depth (Tokioka et al. 1988) improves the simulation of CCEWs, including the MJO, through inhibiting too frequent convections (Wang and Schlesinger 1999; Lee et al. 2003; Lin et al. 2008). Although these simple methods are based on observation and have a positive impact, results are much too sensitive to a single parameter. For example, by changing the parameter α in the method espoused by Tokioka et al. (1988), we can regulate MJO variance by more than factor of two (Lin et al. 2008).

For the triggering process of the present convection scheme, we have followed Jakob and Siebesma (2003)'s

approach. Their method is based on an entraining parcel model, consistent with the cloud model that will be described later in this chapter. The triggering decision for convection is made at the level at which the parcel is saturated. If the vertical velocity of the parcel is positive at that level, convection occurs. To determine the thermodynamic properties (e.g. moist static energy and total water content) and vertical velocity of the rising parcel, Eqs. 6 and 8 are used. All constants are the same as the cloud model except for ε , the fractional entrainment rate, which is prescribed as a function of height (de Roode et al. 2000),

$$\varepsilon \cong c_e \frac{1}{z}, \quad c_e = 0.55, \tag{1}$$

where z is height above the surface.

The surface value of w_u is determined using an empirical formulation suggested by Holtslag and Moeng (1991),

$$w_u(z_1) = \sigma_w(z_1), \tag{2}$$

$$\frac{\sigma_w(z_1)}{w_*} \cong 1.2 \left[\left(\frac{u_*}{w_*} \right)^3 + 0.6 \frac{z}{z_i} \right]^{1/3}, \tag{3}$$

where z_1 represents model's first level, σ_w is the standard deviation of vertical velocity, w_* is the sub-cloud layer vertical velocity scale, u_* is the friction velocity, z is height and z_i is PBL height. Temperature and humidity excesses are added on to the model's first layer (surface layer) values of temperature and specific humidity, using below formulation (Troen and Mahrt 1986)

$$\vartheta_u(z_1) = \bar{\vartheta}(z_1) + b \frac{\overline{w'\vartheta'_s}}{\sigma_w(z_1)}, \quad b = 1, \tag{4}$$

where ϑ is the temperature or specific humidity and $\overline{w'\vartheta'_s}$ the surface flux.

In the current scheme, convection is permitted only if the vertical velocity of the parcel has a positive value when the cloud liquid water is firstly diagnosed—the lifting condensation level. The negative vertical velocity at the lifting condensation level represents stable and/or dry situations within the sub-cloud layer, which prevents the activation of cumulus convection. A convection scheme without a triggering method (e.g. Arakawa and Schubert 1974) implicitly assumes that cumulus convection always occurs when convective available potential energy (CAPE) is positive. In reality, however, deep convection can be suppressed during the period of high CAPE, when rising parcels contain buoyancy which is not enough to penetrate sub-cloud layer. The triggering mechanism reflects PBL influence on cumulus convection.

2.2 Cloud model

The cloud model determines in-cloud properties, such as, the normalized mass flux profile, temperature, specific humidity and cloud liquid water of the rising parcel. We employed an entraining-detraining plume model equations

$$\frac{\partial \eta}{\partial z} = (\varepsilon - \delta)\eta, \quad (5)$$

$$\frac{\partial \theta_u}{\partial z} = -\varepsilon(\theta_u - \bar{\theta}) + S_{\theta_u}, \quad (6)$$

where η is the normalized mass flux, and ε and δ are fractional entrainment and detraining rates respectively. In Eq. 6, the generic variable θ can be moist static energy (h) and total water (q_t). The in-cloud temperature, specific humidity and liquid water are diagnosed using and q_t by the method in Arakawa and Schubert (1974). $\bar{(\)}$ and $(\)_u$ represent the grid mean and updraft parcel value, respectively. S_{θ_u} represents the source or sink term of conserved variables. Here, the simple microphysics for conversion of cloud liquid water to rain drops is a sink term for q_t following Ogura and Cho (1973); that is,

$$S_{q_t} = l_u \left\{ 1 - \exp\left(\frac{-c_{pr}\Delta z}{w_u}\right) \right\}, \quad (7)$$

where l_u is cloud liquid water, $c_{pr} = 0.02 \text{ s}^{-2}$ is a conversion coefficient, Δz is layer depth, and w_u is the updraft vertical velocity. The vertical velocity equation of the updraft parcel is given by (Simpson and Wiggert 1969; Gregory 2001),

$$\frac{1}{2} \frac{\partial w_u^2}{\partial z} = aB_u - b\varepsilon w_u^2, \quad (8)$$

where a and b are constants which are specified here as $a = 1/6$ and $b = 2$. B_u is the buoyancy of the updraft parcel, defined as

$$B_u = \frac{g}{T_v}(T_{v_u} - \bar{T}_v) - gl_u, \quad (9)$$

where g is the gravitational constant, and T_v the virtual temperature. In Eq. 8, the effects of pressure perturbation are implicitly represented as a linear combination of two terms on the right hand side.

Gregory (2001) suggested fractional entrainment rate parameterization based on budgets of cumulus vertical velocity as

$$\varepsilon = \frac{C_\varepsilon ag}{w_u^2} B_u, \quad (10)$$

where C_ε is the conversion factor of the kinetic energy generated by buoyancy to entrained air. A value of 0.25 (0.6) is used for deep (shallow) convection in Gregory (2001).

The effects of buoyancy and vertical velocity on entrainment rate seem to be opposite; a parcel with a stronger vertical velocity (more buoyancy) has a smaller (larger) entrainment rate. It is reasonable, however, to think that the entrainment rate is more strongly dependent on vertical velocity because the (square of) vertical velocity has larger order of magnitude ($O(10^0) \text{ m}^2/\text{s}^2$) than that of buoyancy ($\sim O(10^{-1}) \text{ K}$). A large entrainment rate with a small vertical velocity suggests that the entrainment rate is large near the cloud base and top, where the vertical velocity of a rising parcel is small. This is consistent with entrainment rates that are calculated from cloud resolving model studies (Lin 1999; Cohen 2000; Swann 2001).

Lack of sensitivity to environmental humidity is suggested as a problem of the current convection scheme (Derbyshire et al. 2004) as discussed in Sect. 1. We put the moisture factor in C_ε to account for the sensitivity. Substitution of (10) into (8) results in

$$\frac{1}{2} \frac{\partial w_u^2}{\partial z} = a(1 - C_\varepsilon b) B_u. \quad (11)$$

C_ε plays a key role in the current entraining-detraining plume model by modulating the fractional entrainment rate in (10) and the amount of kinetic energy increase per parcel buoyancy in (11). With a large value of C_ε , an updraft parcel entrains more, and its vertical velocity increases less with the same buoyancy. We assumed a simple dependency of C_ε on environmental humidity, such that

$$C_\varepsilon = \left(\frac{1}{\overline{\text{RH}}} - 1 \right), \quad (12)$$

where, RH is the relative humidity. When C_ε is larger than $1/b$ (currently 0.5), which is equivalent to the condition where $\overline{\text{RH}}$ is smaller than $2/3$, (11) implies that parcel vertical velocity decreases with altitude even if there is positive buoyancy. When buoyancy is negative, C_ε is set to -0.25 to make the parcel rapidly lose its kinetic energy. Note that fixed values of C_ε are used when $\overline{\text{RH}}$ is larger than 99% ($C_\varepsilon = 10^{-2}$) and smaller than 10% ($C_\varepsilon = 10$). The maximum (minimum) value of the entrainment rate is constrained to $10^{-3}(10^{-5}) \text{ m}^{-1}$. The moisture factor is based on the argument that a humid environment favors convective organization (Grabowski 2003). With the moisture factor, it is hard for the cloud parcel to penetrate the dry layer because of stronger mixing with the environment, which will effectively dilute the cloud parcel and give it negative buoyancy. When vertical velocity of the parcel becomes negative, the cloud top level is diagnosed and the convection scheme stops to lift the parcel further.

The fractional detraining rate is treated in a simple manner based on physical argument and previous numerical modeling studies. We assumed that the mass flux is linearly decreasing to zero at cloud top above the

maximum buoyancy level. Bretherton and Smolarkiewicz (1989) suggested that detrainment occurs when parcel buoyancy decreases with height. In numerical modeling studies using a large eddy simulation and a cloud system resolving model on cumulus convection, monotonic decreases of updraft mass flux above a certain level (e.g. Fig. 7 of Cohen 2000) are often observed. Siebesma (1998) and De Rooy and Siebesma (2008) used the same formulation for shallow convection.

$$\delta = \varepsilon + \frac{1}{z_t - z}, \quad z_{B_{max}} \leq z \leq z_t \tag{13}$$

where z_t and $z_{B_{max}}$ are cloud top and maximum buoyancy height, respectively.

2.3 Closure

The closure method determines the strength of convection in a mass flux convection scheme. The closure of the many contemporary deep convection schemes is based on the CAPE or cloud work function, the amount of energy released when the cloud parcel is lifted to the cloud top. It is based on the concept of quasi-equilibrium (Arakawa and Schubert 1974), which assumes the balance between the destabilizing effect of large-scale (which has also longer time scale) phenomena and the stabilizing effect of the ensemble of cumulus convection. Later the strict quasi-equilibrium concept (instantaneous adjustment) has been modified to a relaxed one (Moorthi and Suarez 1992) and widely used now. This kind of closure method seems to be adequate for deeper cumulus convection whose driving force is mainly column instability between the cloud base and top. For the cumulus whose vertical size is small, however, the applicability of closure based on CAPE is questionable. Meanwhile, Neggers et al. (2004) have compared three different closure methods for the diurnal cycle of shallow convection. They have shown in their comparison that the subcloud convective velocity scaling method is superior, in their specific configuration, to both the moist static energy convergence and the CAPE closure methods for shallow convection.

Determining the cloud base mass flux is usually referred to as the closure of mass flux-type convection schemes because it is the only remaining procedure after determining normalized mass flux using the cloud model. A subcloud convective velocity scaling method relates the base mass flux to turbulent kinetic energy in the subcloud layer. And turbulent kinetic energy is represented by a vertical velocity scale of the subcloud layer defined as

$$w_* = \left(\frac{gh \overline{(w'\theta')}}{\theta_{v_0}} \right)^{\frac{1}{3}}, \tag{14}$$

where, h is PBL height, $\overline{(w'\theta')}$ the surface heat flux, θ_{v_0} the surface virtual potential temperature.

In the bulk mass flux convection scheme developed here, a hybrid method is used by combining CAPE closure and a subcloud convective velocity scaling method. It allows for more contribution from CAPE closure (subcloud convective velocity scaling method) for deeper (shallower) convection in determining cloud base mass flux. The clouds which have their top below the minimum moist static energy level are regarded as shallow convection and a subcloud convective velocity scaling method is used as closure for those clouds. CAPE closure is used only if the cloud top is higher than the level of minimum moist static energy level. The higher the cloud top is, the closer the cloud base mass flux is to that of CAPE closure.

For the base mass flux for deep convection, we follow Nordeng (1994) as,

$$M_b \text{ (deep)} = \frac{\text{CAPE}}{\tau \int_{\text{cloud}} \left(\frac{1+\varepsilon\bar{q}}{c_p T_v} \frac{\partial s}{\partial z} + \varepsilon \frac{\partial \bar{q}}{\partial z} \eta dz \right)} \tag{15}$$

$$\text{CAPE} = \int_{\text{cloud}} B dz \tag{16}$$

where s is the dry static energy, τ the convective adjustment time scale. The relaxation time scale in CAPE closure depends on ‘eddy overturning time scale’, which proportions an amount of time needed when the hypothetical air parcel travels from the surface to the cloud top.

We adopted Grant (2001)’s formulation of the base mass flux for shallow convection,

$$M_b \text{ (shallow)} = 0.03 \times w_* \tag{17}$$

where, w_* is the convective velocity scale of the subcloud layer, which is obtained from the planetary boundary layer (PBL) process. The hybrid cloud base mass flux is then,

$$M_b = \frac{1}{D} (D_1 M_b \text{ (shallow)} + D_2 M_b \text{ (deep)}) \tag{18}$$

where, D is cloud depth, D_1 the depth between cloud base and minimum MSE level, D_2 the depth between the minimum MSE level and the cloud top ($D_2 = 0$ and $D = D_1$, if $D_2 < 0$).

Finally, the cloud mass flux is,

$$M = \eta M_b \tag{19}$$

3 Models and experiments

3.1 General circulation model and single column model

The GCM used in this study is the Seoul National University GCM (SNUGCM). A single column version of the SNUGCM is used as a SCM in Sects. 4 and 5. The deep

convection scheme is a simplified version of the relaxed Arakawa-Schubert scheme (hereafter, RAS; Numaguti et al. 1995). The large-scale condensation scheme consists of a prognostic microphysics parameterization of total cloud liquid water (Le Treut and Li 1991) with a diagnostic cloud fraction parameterization. A non-precipitating shallow convection scheme (Tiedtke 1984) is also implemented in the model for the mid-tropospheric moist convection. The boundary layer scheme is a non-local diffusion scheme based on Holtslag and Boville (1993), while the land surface model is from Bonan (1996). Atmospheric radiation is parameterized by a two-stream k distribution scheme, as in Nakajima et al. (1995). Other details of the model physics are described in Lee et al. (2001, 2003).

3.2 Cloud resolving model

The CRM used is the Goddard Cumulus Ensemble model (GCE; Tao and Simpson 1993; Tao et al. 2003). The GCE model solves non-hydrostatic governing equations with sophisticated cloud microphysics. The prognostic variables of the governing equations are horizontal and vertical velocities, potential temperature, perturbation pressure, turbulent kinetic energy, and mixing ratios of all hydrometeors. Two kinds of liquid water and three-category ice-phase hydrometeors are used in the cloud microphysics (Lin et al. 1983; Rutledge and Hobbs 1984). The sub-grid scale turbulence scheme is based on Klemp and Wilhelmson (1978). The GCE uses the radiation scheme of Chou and Suarez (1999) for shortwave and Chou and Suarez (1994) for longwave radiation, respectively. Previous studies have shown that the GCE model simulates tropical cloud systems in a reasonable manner. (Johnson et al. 2002). In this study, a 2-dimensional version of the model with cyclic boundary conditions in a 256 km domain size is used. As described later, three different horizontal grid sizes (125, 250 and 500 m) are tested and output from 500 m resolution model is mainly used here. The vertical resolution is about 80 m near the surface, which gradually increases with height up to about 700 m near the 10 km level.

3.3 Experimental design

Recently, the Precipitating Cloud Systems Working Group (PCS WG, Moncrieff et al. 1997) of the Global Energy and Water Cycle Experiment (GEWEX) Cloud System Study (GCSS) conducted a case-study using various modeling frameworks, such as, CRM, GCM (include climate and numerical weather prediction models), and SCM (Petch et al. 2007; Willett et al. 2008). The GCSS aims to support the development of new parameterizations of all cloud-related processes for large-scale models (Randall et al.

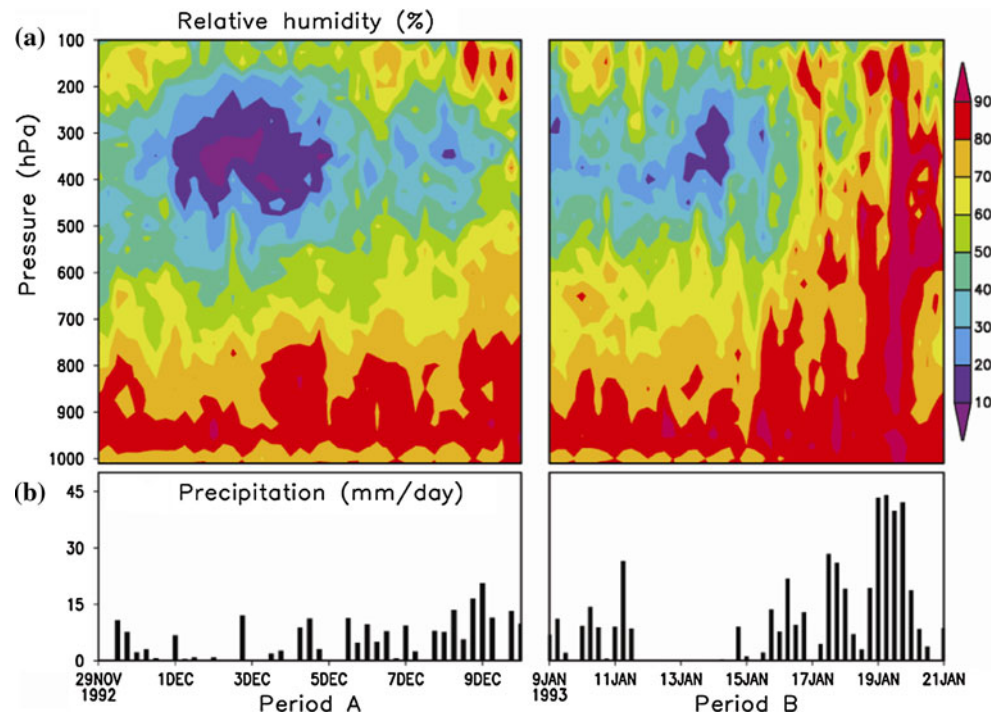
2000). The theme for a recent case study of the PCSWG is ‘modeling the suppressed and active convection’. It is of interest to correctly simulate suppressed and active periods of tropical convection because the successful simulation of suppressed, active and transition periods of tropical convection is crucial in the simulation of tropical sub-seasonal variability, such as the MJO. The period for the case study which focuses on the suppressed and active periods of convection was chosen from the Tropical Ocean and Global Atmosphere-Coupled Ocean-Atmosphere Response Experiment (TOGA-COARE, Webster and Lukas 1992) period.

Two periods were selected following PCSWG’s strategy. They are period A (29 November–10 December 1992) and B (9 January–21 January 1993). These periods included suppressed and active convective regimes as well as the transition between them. Figure 1 shows observed relative humidity and budget derived precipitation during the two periods. At a first glance, heavy precipitation prefers to occur during the moistened period (e.g. 19 January). The Global Energy and Water Cycle Experiment (GEWEX) Cloud System Study (GCSS) provides the initial conditions and forcing data for SCM and CRM simulations. We used the horizontal and vertical advection of potential temperature and the specific humidity and vertical profile of zonal and meridional winds for the SCM and CRM experiments (Ciesielski et al. 2003, http://tornado.atmos.colostate.edu/togadata/ifa_data.html). The data represent an average over the TOGA-COARE intensive flux array (IFA), a region of about 400 km by 250 km centered on 2°S 155°E. The sea surface temperature (SST) is prescribed as an observed value while the surface fluxes are calculated using the model’s own surface model. Therefore, the integration of the SCM is identical to that of atmospheric GCM (AGCM) except for the advection term, which is replaced by prescribed forcing for temperature and specific humidity and nudging toward observed values for the zonal and meridional winds.

4 Moisture sensitivity in an idealized experiment

To test moisture sensitivity of the current convection scheme, an idealized experiment is conducted in a SCM framework. In Derbyshire et al. (2004) experiment, temperature and humidity are relaxed toward specified profiles to simplify the complex problem of feedback between convection and large-scale circulation. We adopt a similar method but we integrate a single column version of GCM for just one time step using the specified profiles as initial conditions. Therefore, there is no feedback from convection to environment and we only aim to see the response of convection to the different environmental conditions. Also,

Fig. 1 **a** Relative humidity and **b** precipitation observed during selected period from total TOGA-COARE IFA period. *Left (right)* panels shows period A (**b**). Units for relative humidity and precipitation are % and mm day^{-1} , respectively



we use the temperature and specific profiles from observations, while Derbyshire et al. (2004) used idealized conditions.

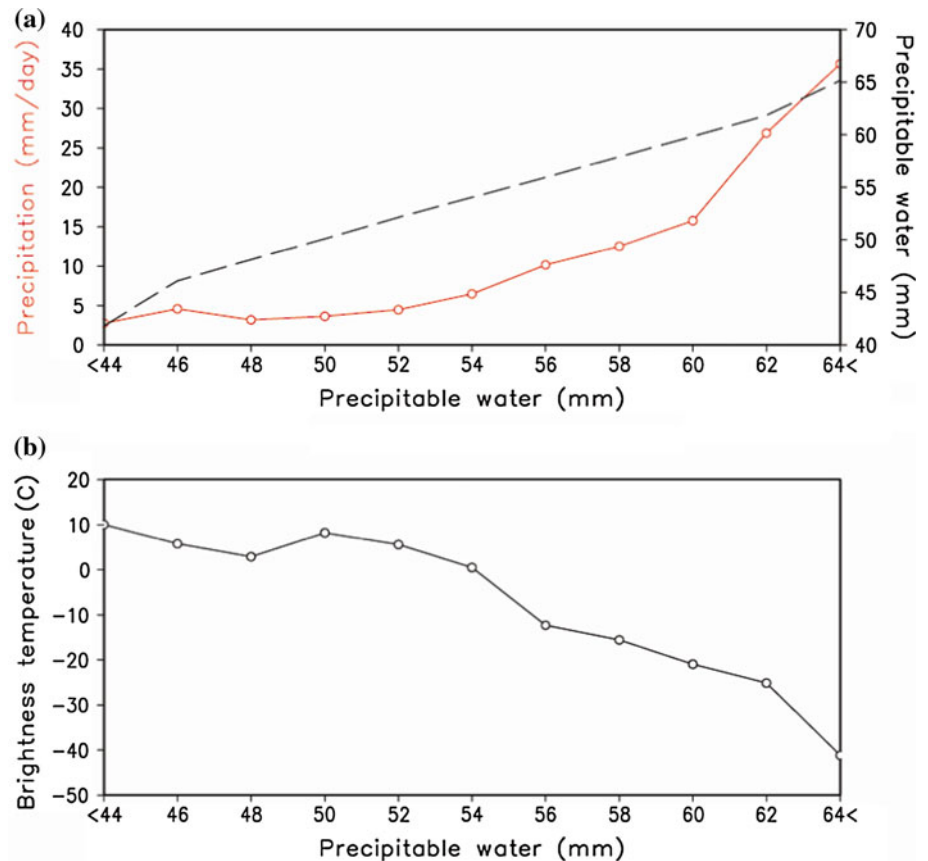
Composites are made for all input variables to SCM, which are zonal/meridional wind, temperature, specific humidity and surface pressure, based on precipitable water (PW) using the TOGA-COARE IFA data. Compositing thermodynamic profiles based on PW is inspired by a recent observational study (Holloway and Neelin 2009), which showed the relationship between precipitation and PW. Figure 2a shows composited precipitation and PW. While PW increases linearly, precipitation is enhanced rapidly after some critical PW (54 mm), consistent with Holloway and Neelin (2009) results. Composited brightness temperature, which roughly represents cloud top height, is shown in Fig. 2b. A high PW, strong precipitation regime has lower brightness temperature, suggesting deep convection occurs in that regime. Composited moist static energy, saturation moist static energy and relative humidity are shown in Fig. 3a and b. A high PW amount is accompanied by moist atmosphere throughout the troposphere (Fig. 3b). Note that the saturation moist static energy for each category is not very different (Fig. 3a), implying that the variability of temperature is relatively small compared to that of specific humidity. The moist static energy curves show that the moist static stability varies much from most stable condition in most dry atmosphere, to most unstable condition in most wet column. When we prescribe temperature and specific humidity profile to SCMs, specific humidity amounts below 850 hPa

level are adjusted so as the columns have fixed environmental relative humidity. The fixed value is 85% at 850 hPa and 90% at surface, with linearly increasing condition from 850 hPa to the surface. The modification of environmental specific humidity is to activate cumulus convection in all categories and examine environmental humidity impacts on simulated convection.

Figure 4 shows updraft mass flux, as a proxy of convective activity, simulated by SCMs using two different convection schemes. In RAS (Fig. 4a), cloud top is the same in all experiments, representing inadequate sensitivity of convection to environmental moisture. This is mainly because it is assumed in RAS that all kinds of cumulus clouds, characterized by their top height, potentially exist (Arakawa and Schubert 1974). Practically, RAS tests all cloud tops (types) above cloud base. When a cloud top level is specified as neutral buoyancy level, entrainment rate between cloud bottom and top is determined based on in-cloud properties at cloud bottom and environmental conditions at cloud top. In this framework, deep clouds, which have small entrainment rate and therefore are relatively less affected by environmental condition, could be generated easily.

On the other hand, BMF (Fig. 4b) simulates shallower and weaker updraft mass flux in drier environments and vice versa, similar to the modulation of convection by environmental moisture condition shown in previous observational and modeling studies (Sherwood 1999; Ridout 2002; Derbyshire et al. 2004; Takayabu et al. 2006; Holloway and Neelin 2009). BMF simulates deep

Fig. 2 Compositing
a precipitation (*solid*),
precipitable water (*dashed*), and
b brightness temperature based
on precipitable water. TOGA-
COARE IFA data is used. Units
for precipitation and
precipitable water are
 mm day^{-1} , and mm ,
respectively. Unit of brightness
temperature is $^{\circ}\text{C}$



convection only if the column is moist enough (Fig. 4b), because the entrainment rate (Eq. 10) is enhanced and the kinetic energy transfer efficiency (Eq. 11) is reduced in dry conditions. BMF produces a low-heavy mass flux (Fig. 4b) in dry cases, while it becomes top-heavy in moister environments. Note that the maximum value of mass flux appears in relatively higher levels (e.g. about 400 hPa), especially for deep convections. The top-heavy profiles of the mass flux make diabatic heating profile top-heavy (Fig. 6).

Several sensitivity experiments are conducted using BMF for a better understanding on factors which are important to simulate proper cloud top height sensitivity to environmental moisture. The results of sensitivity experiments are shown in Fig. 5. In EXP1 (Fig. 5a), C_{ε} in (12) is fixed to 0.3 to turn off the effect of environmental relative humidity on the entrainment rate. To remove dependency of the entrainment rate on parcel buoyancy and vertical velocity, we set ε in Eq. (10) to $5 \times 10^{-4} \times C_{\varepsilon}$ in EXP2 (Fig. 5b). Therefore, the entrainment rate at a level is determined solely by environmental relative humidity of the level in EXP2. When dependence on relative humidity is removed from the formulation of entrainment rate (EXP1), cloud top pressures are lower than 200 hPa in most cases (Fig. 5a). And, when parcel buoyancy and

vertical velocity are not considered in entrainment rate determination, the difference between mass fluxes in different moisture is reduced (Fig. 5b), although cloud top varies in a similar manner to control. Therefore, it seems that both environmental relative humidity and parcel buoyancy and vertical velocity terms are needed to simulate proper sensitivity of cloud top and strength of convection to environmental moisture condition.

In EXP3 and EXP4, to examine the impact of the closure method, only one method is used instead of the hybrid method in Eq. (18). Only the CAPE closure (the subcloud vertical velocity scaling closure) is used in EXP3 (EXP4). In Fig. 5c, the CAPE closure is generally able to produce the variation of base mass flux according to moisture condition, shown in Fig. 4b, except for the shallowest convection. With only the CAPE closure, the shallowest convection has too strong (Fig. 5c) mass flux because of short eddy overturning time scale. When only the subcloud vertical velocity scaling closure is used (Fig. 5d), mass fluxes are too weak overall (scale is different from other panels) and the base mass fluxes in different circumstances are not clearly distinguished. Therefore, the hybrid approach in closure in BMF has a positive impact on simulating proper sensitivity of convective activity to environmental humidity. By fixing the cumulus adjustment

Fig. 3 Compositing **a** moist static energy (*solid*), and saturation moist static energy (*dashed*), and **b** relative humidity based on precipitable water. TOGA-COARE IFA data is used. Unit for moist static energy and relative humidity are kJ kg^{-1} and %, respectively

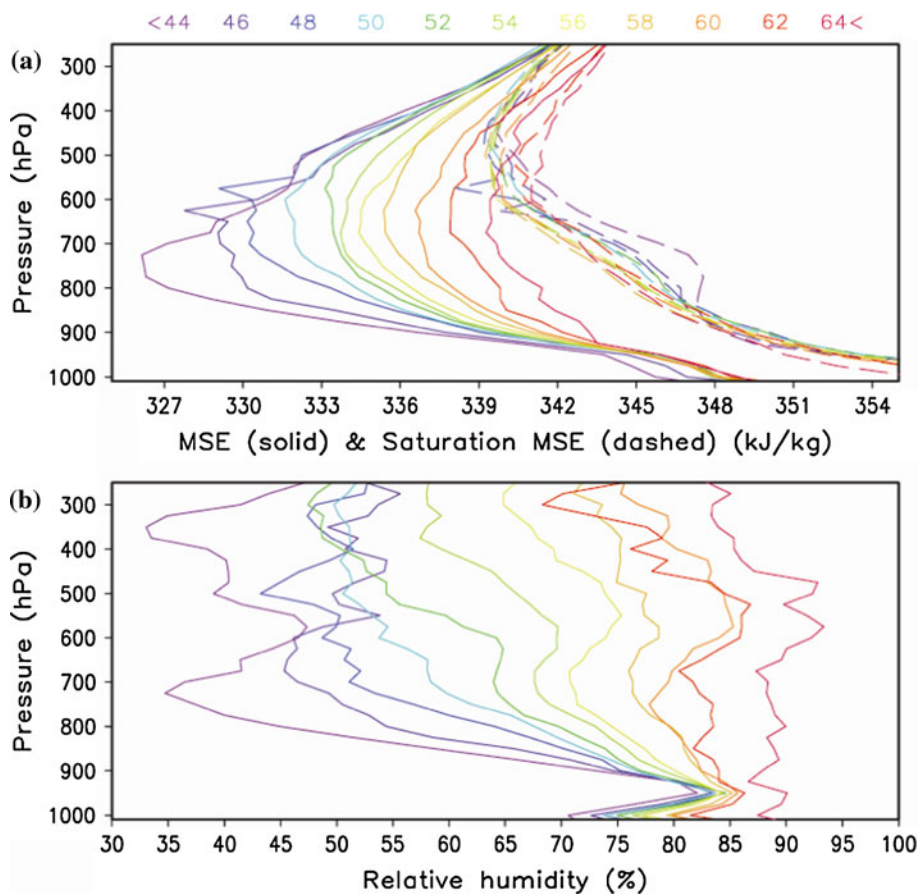
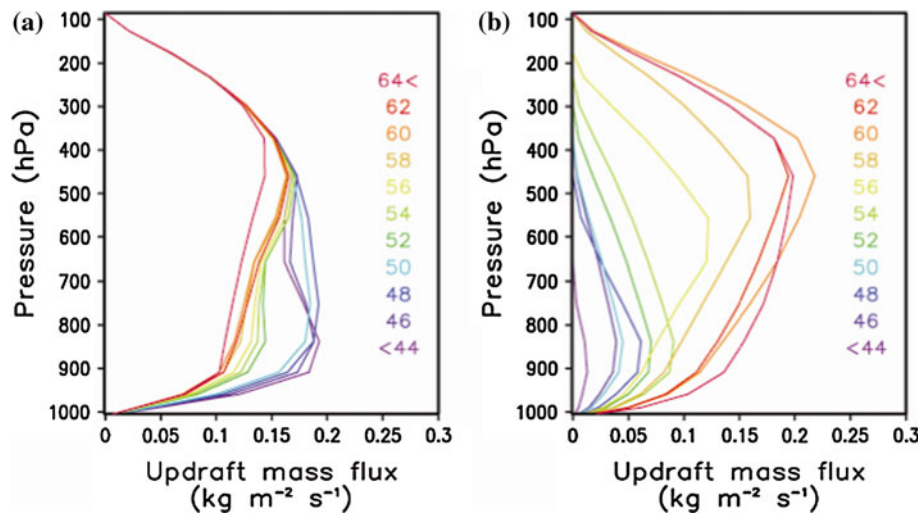


Fig. 4 The updraft mass flux simulated by **a** RAS, and **b** BMF. Different colors show different precipitable water amounts used in single time step experiment. Unit of mass flux is $\text{kg m}^{-2} \text{s}^{-1}$

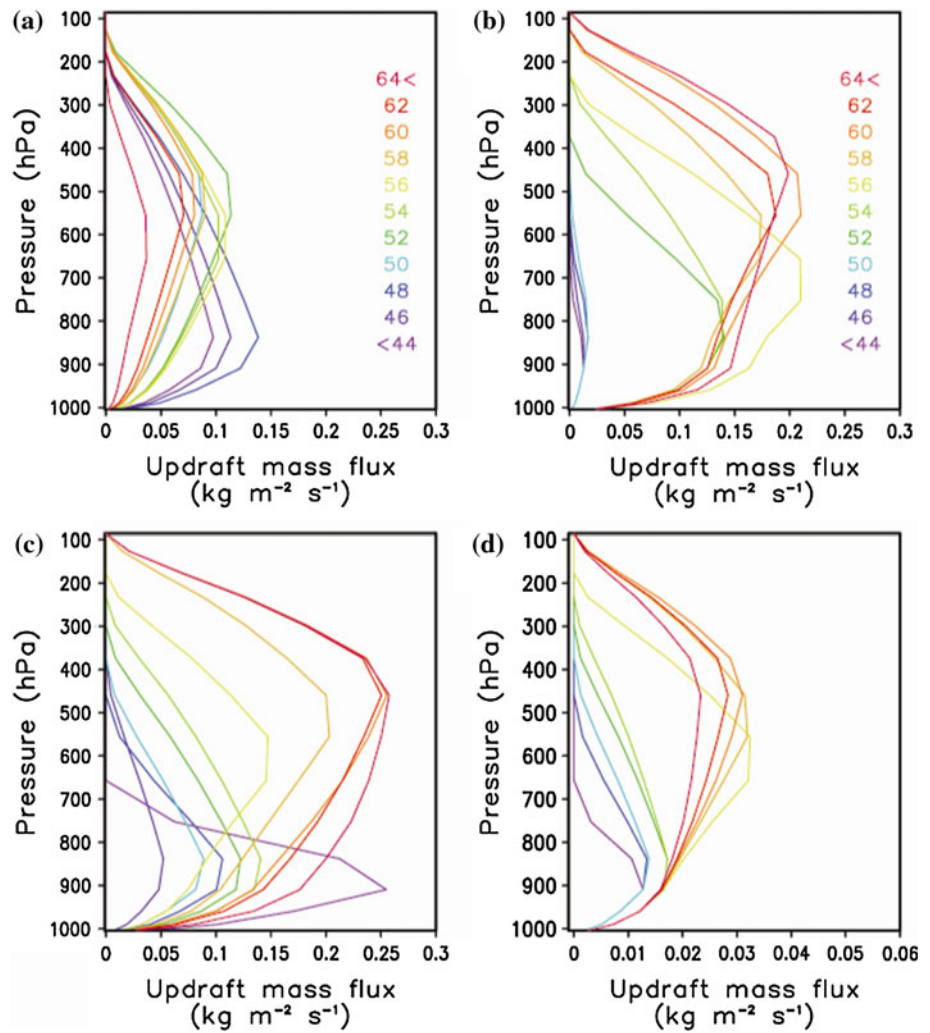


time scale as constant, we could roughly measure the cloud adjustment time scale defined as a function of eddy overturning time scale in BMF, whereupon it is found to be between 2,400 and 4,800 s (not shown).

Figures 6 and 7 show the effects of convection on environment in the single time step experiments. The tendency of potential temperature produced by two convection schemes is presented in Fig. 6. Because potential

temperature is usually increasing with height, the subsidence in environment, which compensates the upward mass flux within cloud, produces heating in the most layers. Meanwhile, evaporation of detrained cloud water and falling precipitation, and a compensating upward motion by downdraft modifies the heating field. RAS generates nearly identical heating for all cases (Fig. 6a), because both environmental temperatures and mass flux profiles are

Fig. 5 The updraft mass flux simulated in different experiments. **a** EXP1, **b** EXP2, **c** EXP3, and **d** EXP4. Different colors show different precipitable water amounts used in single time step experiment. Unit of mass flux is $\text{kg m}^{-2} \text{s}^{-1}$



similar in all cases. In the case of BMF, heating (Fig. 6b) is consistent with mass flux (Fig. 4b); wetter cases have a deeper and stronger heating and vice versa. Note that in BMF, the structures of heating are relatively top heavy, especially for the three wettest columns. This is because the maximum buoyancy levels, from which plume starts to detrain, are in higher altitudes in those columns, with lower entrainment rate.

Figure 7 shows moistening profiles represented by two convection schemes in different PW conditions. In the most humid case, both schemes have similar effects on the environment; convection dries the troposphere except for near the cloud top level, in which cloud water is detrained. RAS dries heavily the lower troposphere (near 800 hPa) even when the column is dry and relative humidity is low. By formulating entrainment rate as a function of environmental relative humidity and parcel buoyancy and vertical velocity, and by using hybrid closure method, BMF simulate shallower and weaker convection in drier conditions. The shallower and weaker convection less warms and dries

the environment, especially the lower troposphere. The impact of the difference between BMF and RAS shown in Figs. 6 and 7 will be examined in the following section within SCM and GCM frameworks.

The convective precipitation produced in each experiment is shown in Fig. 8. The sensitivity of precipitation to environmental moisture condition, which can be measured by either the saturation deficit or PW, is suggested as a prerequisite for proper simulation of equatorial large-scale waves (Raymond 2001). BMF (Fig. 8, red line) captures the strong sensitivity of convective precipitation to environmental moisture when PW is greater than 52 mm (similar to observed value from which precipitation increases rapidly). RAS (blue line) lacks the dependency of precipitation on PW, precipitation is even greater in dry cases (52 mm shows maximum precipitation), which is consistent with its simulation of the mass flux (Fig. 4a). The sensitivity produced by BMF is similar to the observed feature, which is shown in Fig. 2a. The results given in this section show that BMF is able to capture a proper

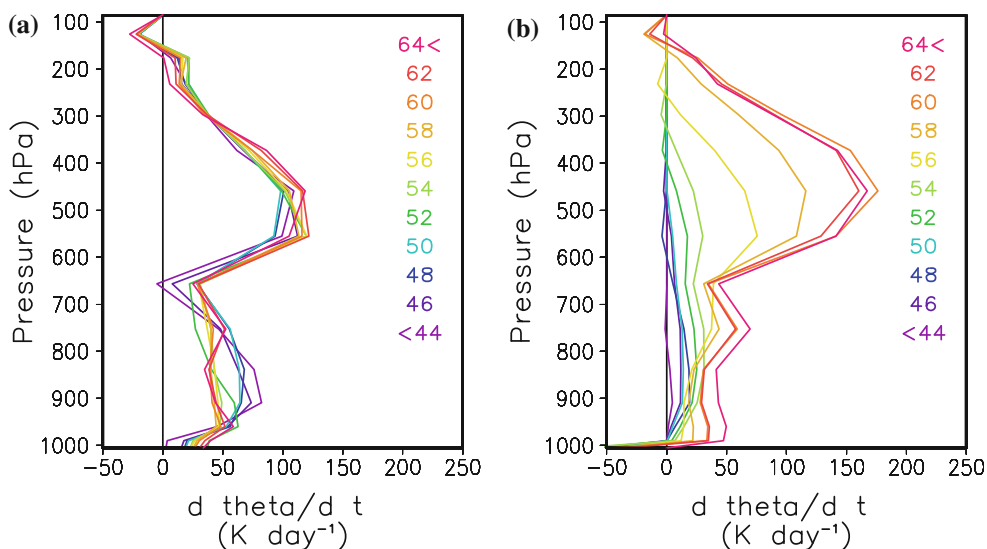


Fig. 6 The tendency of potential temperature simulated by **a** RAS, and **b** BMF. Different colors show different precipitable water amounts used in single time step experiment. Unit is $K day^{-1}$

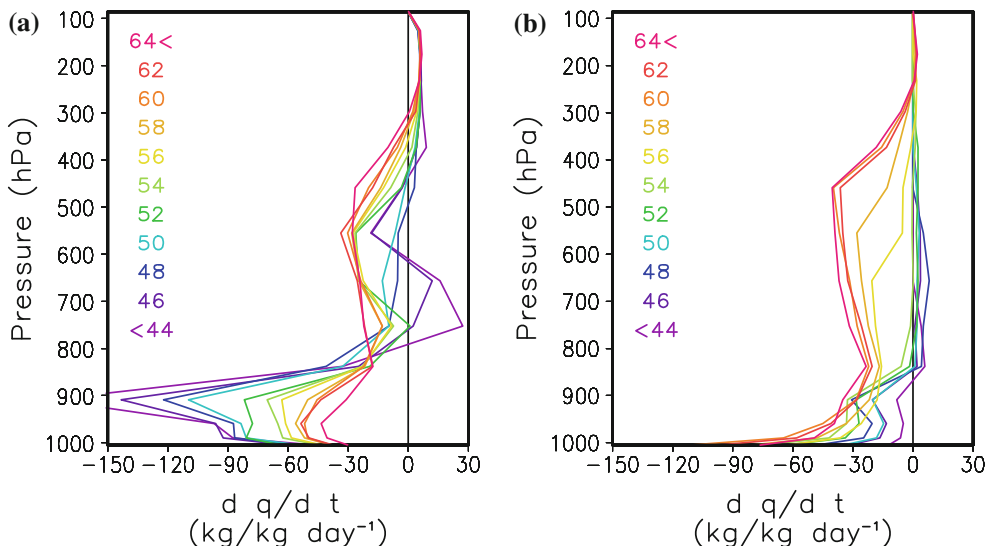


Fig. 7 Same as Fig. 6, except for the tendency of specific humidity

sensitivity of convection to environmental moisture, which is not adequately represented in RAS. The key factors for regulating cloud top height and strength of convection according to environmental moisture are also shown as the dependence of entrainment rate on environmental and cloud properties and the hybrid closure method.

5 Performance of the bulk scheme

In this section, the performance of the current convection scheme is examined in SCM and GCM frameworks. In SCM framework, observed tendencies of temperature and

specific humidity are given to column to see the response of the model physics, including cumulus parameterization. A long-term (10 years) integration of AGCM is conducted with two different convection schemes to see (i) whether BMF convection scheme works properly in the global model, and (ii) impacts of convection scheme on the simulation of the intraseasonal variability in the tropics.

5.1 Single column model

Before comparing the SCM results with observation and the CRM simulation, the problem of the default convection scheme (RAS) of SNUGCM is first diagnosed. Figure 9

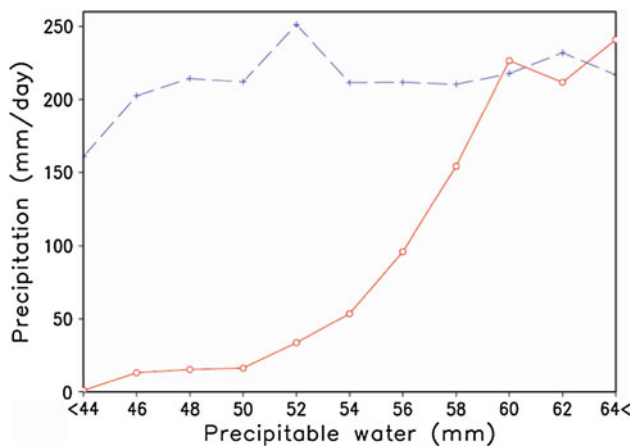


Fig. 8 The precipitation simulated in different precipitable water circumstance by RAS (blue) and BMF (Red). Unit is mm day⁻¹

shows the relative humidity bias and precipitation simulation over two selected periods described in Sect. 3.3. Although SCM with RAS simulates total precipitation relatively well (Fig. 9, bottom panels), relative humidity has a systematic bias, that is, a dry lower troposphere and a wet upper troposphere. The bias in relative humidity is mainly from the specific humidity bias, in particular in the lower troposphere (not shown). This problem is not just a symptom of SCM, and it reflects the bias in climate simulation over the tropics. Figure 10 shows the difference between the area-averaged relative humidity from the 40-year European Centre for Medium-Range Weather Forecasts (ECMWF) Re-Analysis (ERA40, Uppala et al. 2005) and atmospheric model intercomparison project (AMIP)-type simulation of SNUGCM with a RAS convection scheme. For AMIP-type simulation, SNUGCM is integrated using observed sea-surface temperature as a boundary condition for the period of 1999–2008, from initial condition generated using the National Center for Environmental Prediction/National Center for Atmospheric Research (NCEP/NCAR) reanalysis. Time-averaged, vertical profile of relative humidity from ERA40 for the period of 1979–2001 is compared to that from 10-year AGCM simulation in Fig. 10. When relative humidity is averaged over the TOGA-COARE IFA area (solid), the bias is similar to that shown in the SCM experiment. Furthermore, the similar structure of bias appears in tropics-averaged relative humidity (dashed), suggesting this bias is typical problem of the model in the tropics. The bias is mainly because RAS poorly simulates sensitivity to lower tropospheric moisture, as shown in the previous section. A similar problem of a different convection scheme is shown in Thayer-Calder and Randall (2009) for the Community Atmosphere Model (CAM) version 3.0. They showed that a lack of coupling between convection and environmental relative humidity results in the dry mid to lower

troposphere in CAM3.0. In SNUGCM, incorrect simulation of the interaction between convection and environmental moisture in RAS causes systematic bias of the specific humidity in both SCM and AGCM simulations.

We now focus on the updraft mass flux and relative humidity simulations of RAS and BMF. Figure 11 shows the updraft mass flux simulated by the GCE model for the period A. Three different horizontal resolutions (125, 250 and 500 m) are tested. It is shown that the evolution of mass flux over time simulated in CRM is not significantly dependent on horizontal resolution, although some minor differences (e.g. the earliest deep convection only appears at 125 m resolution) are observed. We use 500 m resolution model results below for computational (simulation of period B) and data handling efficiency. Note that GCE simulates the amount of rainfall similar to observation during both periods (not shown).

Figure 12 compares the updraft mass flux simulated by GCE, and two SCM simulations with BMF and RAS. From the GCE output, the updraft mass flux is calculated with 10 min interval by averaging all upward mass flux when the vertical velocity is greater than 0 m/s and the grid contains hydrometeors greater than a critical value (i.e. 1% of saturation specific humidity). Then mass fluxes are averaged into 6 hourly data for convenience of comparison. A gradual increase of cloud top height (Fig. 12a, top of updraft mass flux is regarded as cloud top here) with a moistening of the troposphere (Fig. 13b) is simulated in GCE after 1 December 1992 during period A. In contrast to GCE, the mass flux simulated by RAS has weak signal of gradual growth shown in CRM. Also, relative humidity simulated by SCM with RAS shows the dry bias in the lower layers (Fig. 13d). BMF produces a more realistic—similar to observation and CRM simulation—updraft mass flux and relative humidity (Fig. 12b and 13c). The gradual increase of cloud top height and the strengthening of convective activity from 1 December 1992 is captured in BMF. Furthermore, the growth of cloud top height after 1 December 1992 is accompanied by moistening of the troposphere, as in the observation and GCE. BMF doesn't have the severe dry bias in the lower troposphere, unlike RAS (Fig. 13c). The difference between BMF and RAS is similar in the period B; the gradual increase of cloud top and strengthening of mass flux is better simulated in BMF (Fig. 12, right panels).

Tendency of specific humidity by convection scheme is shown in Fig. 14 to provide a possible reason for difference between RAS and BMF in simulations of the relative humidity. In general, RAS nearly always dries the lower (below 600 hPa) troposphere (Fig. 14b), while BMF moistens there when it is dry. The difference is clearly seen when we look at a specific time domain, which is from 1st to 3rd of December 1992 in period A. This time domain is

Fig. 9 **a** Relative humidity bias and **b** precipitation observed and simulated by single column model during selected period A (left) and B (right). Units for relative humidity bias and precipitation are % and mm day⁻¹, respectively

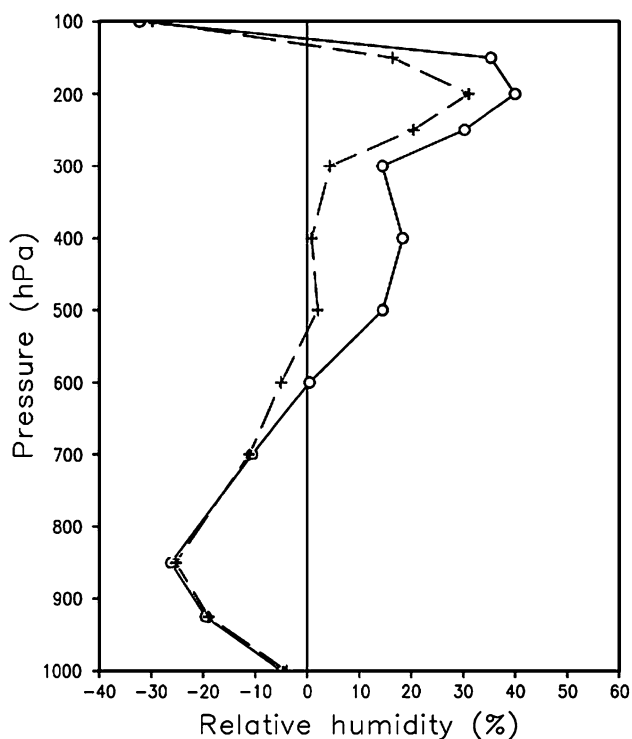
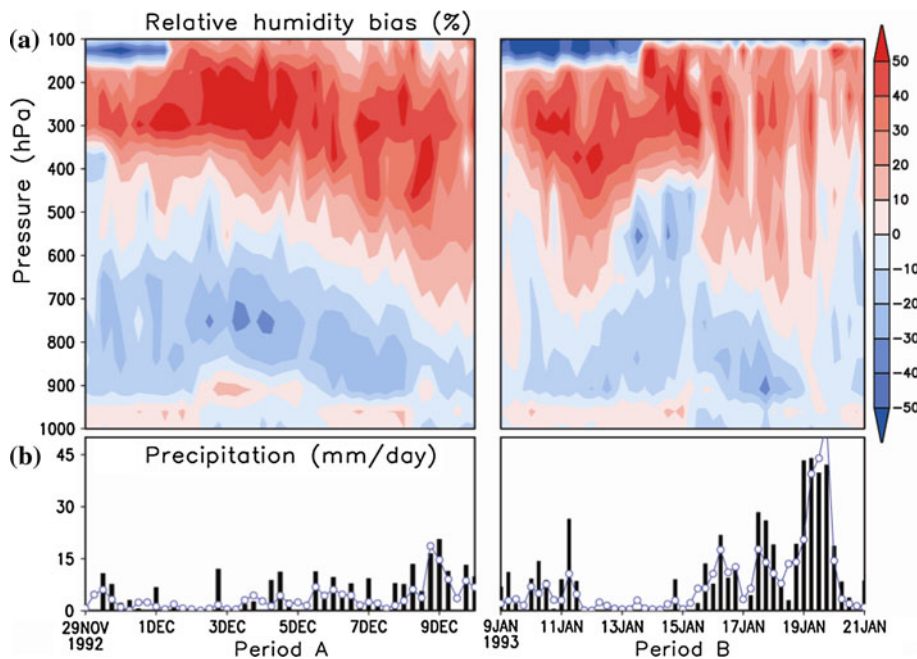


Fig. 10 Relative humidity bias of SNU AGCM averaged over near TOGA region (150–160°E, 5°S–Eq; solid line) and deep tropics (0–360°E, 10°S–10°N averaged; dashed line). Unit is %

characterized by most dry phase during period A for both simulations, in terms of relative humidity below 600 hPa. The RAS dries out the dry layers, so the lower troposphere remains dry (Fig. 13d). In contrast, BMF moistens the lower troposphere in this period (Fig. 14a), after which the

dryness is gradually recovered (Fig. 13c). The different responses of BMF and RAS to similar environmental condition are consistent to the results shown in previous section. The dry bias in the lower troposphere with RAS is due to the lack of the moisture sensitivity of RAS, which simulate deep convection and dries out the low troposphere heavily in dry conditions. This bias is improved in BMF by improving the sensitivity of convection to environmental moisture condition, through strengthening the interaction between environment and cloud. By formulating the entrainment and detrainment in terms of cloud and environment variables in a proper way, BMF makes the interaction between the cloud and environment in a more effective and proper way.

5.2 The effects of convection scheme in GCM simulation

The results of AGCM simulations with BMF and RAS convection schemes are presented in this section. The AGCMs are integrated for 10 years (1999–2008) by prescribing observed sea surface temperature. In this paper, only limited results are shown because the full analysis of AGCM simulations is beyond the scope of the current study.

Figure 15 shows annual mean precipitation of the Global Precipitation Climatology Project (GPCP, Huffman et al. 2001) observation data and AGCM with two different convection schemes for 1999–2008 periods. Both simulations are able to reasonably capture prominent band-like structures in observation, such as, ITCZ and the south Pacific convergence zone (SPCZ). Mean precipitation over

Fig. 11 The updraft mass flux simulated by GCE model for the period A. **a** 125 m, and **b** 250 m, **c** 500 m resolution is used. Unit of mass flux is $\text{kg m}^{-2} \text{s}^{-1}$

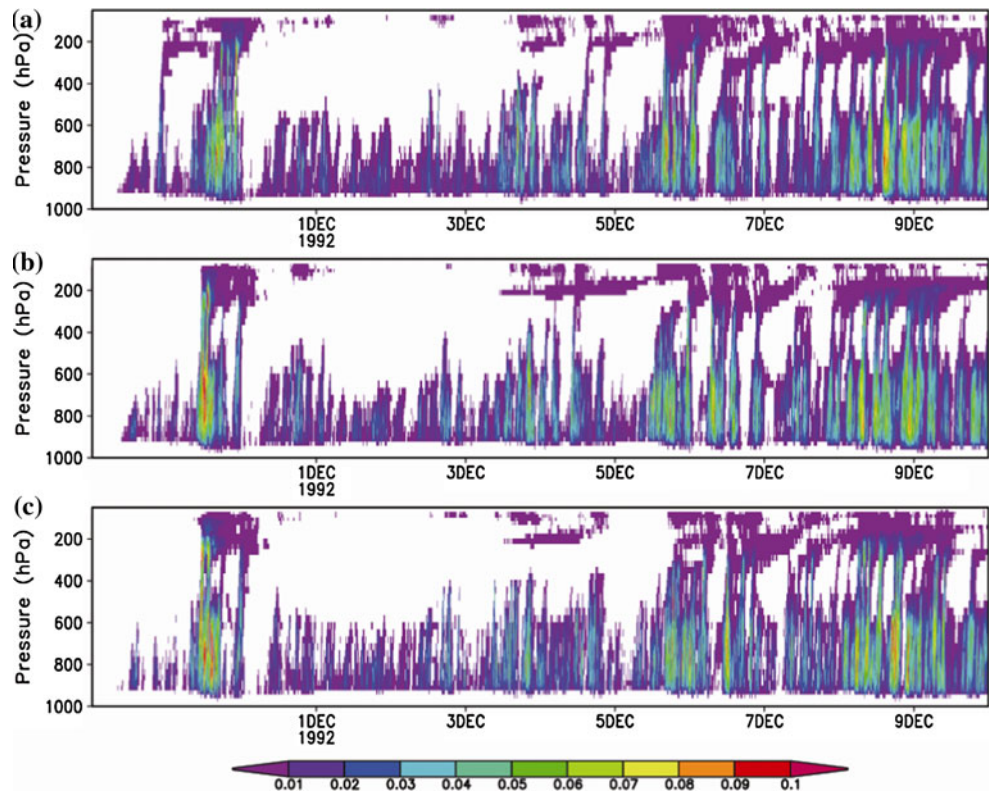
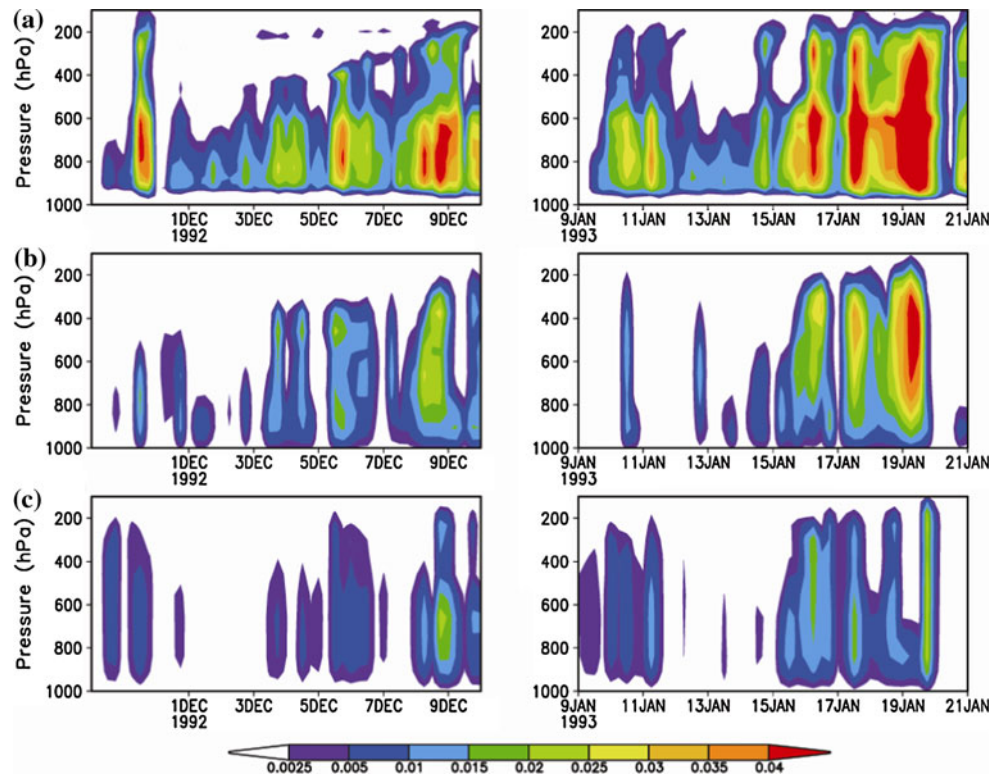


Fig. 12 Updraft mass flux simulated by **a** GCE, **b** SCM with BMF, and **c** SCM with RAS during period A (*left*) and B (*right*). Unit is $\text{kg m}^{-2} \text{s}^{-1}$



the eastern Indian Ocean, however, is commonly not well simulated. Also, RAS and BMF produce excessive precipitation over Indian monsoon region compared to

observation. BMF shows additional wet bias over the northwest Pacific and SPCZ regions. It is shown in Wang et al. (2005) and Wu et al. (2006) that observed relationship

Fig. 13 Relative humidity during period A. **a** observation, **b** GCE, and **c** SCM with BMF, and **d** SCM with RAS. Unit is %

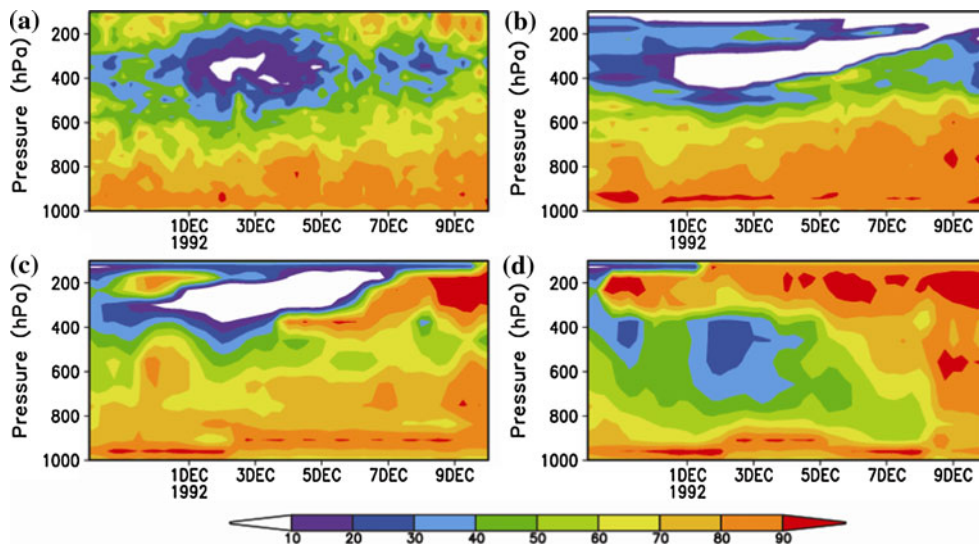
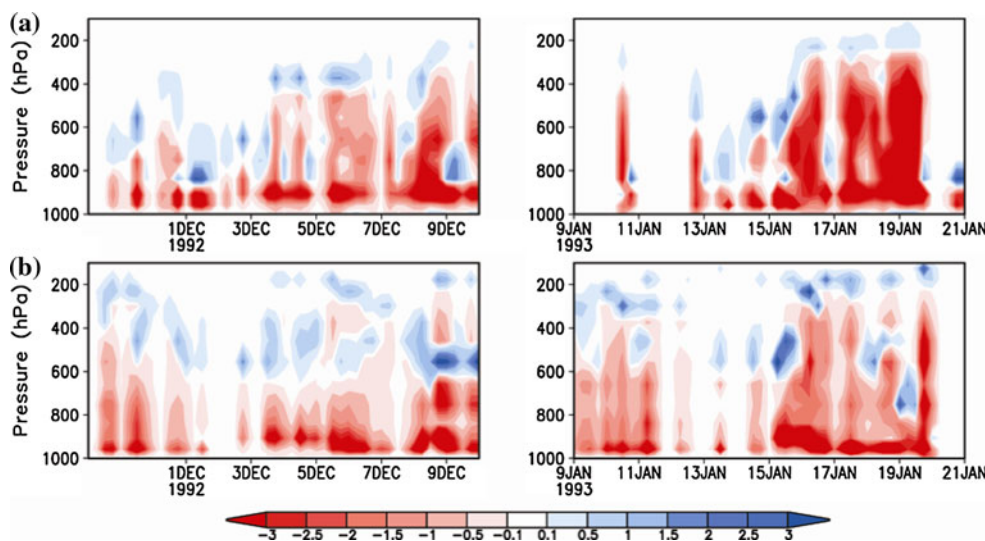


Fig. 14 Tendency of specific humidity by convection scheme during period A (left) and B (right). SCM simulations with **a** BMF, and **b** RAS. Unit is $g\ kg^{-1}\ day^{-1}$

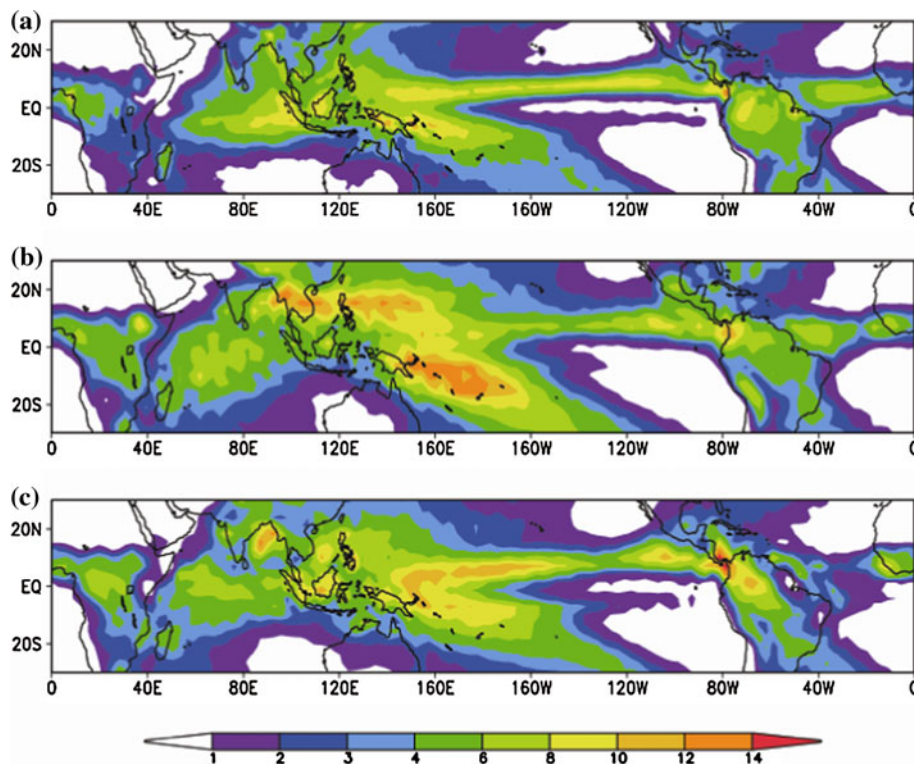


between sea surface temperature and precipitation over the northwest Pacific region is hardly captured in AGCM simulations. And Stan et al. (2010) showed that excessive precipitation over the west Pacific during boreal summer in the super parameterization CAM (Khairoutdinov and Randall 2001) is reduced when the model is coupled to an ocean model. Consistent to Stan et al. (2010)’s results, the wet bias over the northwest Pacific and SPCZ regions is significantly reduced in our preliminary results from ocean–atmosphere coupled GCM (not shown), suggesting that the bias partly comes from the lack of air–sea coupling.

To show the simulation capability of intraseasonal variability, November–April lag–longitude diagram of 10°S–10°N averaged intraseasonal 850 hPa zonal wind anomalies correlated against to the west Pacific reference point in displayed in Fig. 16. Reference point is obtained by averaging 20–100 day band pass filtered 850 hPa zonal wind over the 155–160°E, 5°S–5°N domain. The tropospheric

zonal winds from the NCEP/NCAR reanalysis data (Kalnay et al. 1996) is regarded as observation. In observation, lag–correlation diagram shows an eastward propagation of lower level zonal wind travelling all around the globe (Fig. 16a). The speed of propagation is slower over the Indian Ocean and faster over the central and east Pacific. In RAS, the eastward propagating feature of 850 hPa zonal wind in intraseasonal time scale is not captured. Rather, it produces standing (west Pacific) and westward propagating (in the Indian Ocean) signal. On the other hand, in BMF, eastward propagating signal becomes prominent over the whole longitudes, although the difference in phase speed between Indian Ocean and central/eastern Pacific is not well captured. Our results from AGCM simulations suggests that the strengthening of the cloud–environment coupling in BMF, which improves moisture sensitivity of convection throughout all vertical layers, results in improved simulation of the sub–seasonal variability in the tropics.

Fig. 15 Annual mean precipitation averaged over the period 1999–2008. **a** GPCP, **b** BMF, and **c** RAS. Unit is mm day^{-1}



6 Summary and concluding remarks

A bulk mass flux convection scheme has been developed and evaluated in SCM and GCM frameworks by observation and a cloud resolving model simulation data. Based upon Tiedtke (1989)'s bulk mass flux framework for updraft plumes, the triggering, entrainment/detrainment rate modeling, and closure methods are revised. We adopted the triggering method of Jakob and Siebesma (2003), which enables direct interaction between the sub-cloud layer and convection by using a parcel model. Cloud parcel properties (i.e. moist static energy, total water amount and vertical velocity) from the surface layer to cloud top level are treated in a consistent manner by solving an entraining updraft and vertical velocity equations. A key parameter in these equations is the entrainment rate, which is prescribed in the sub-cloud layer as a function of height and is determined based on parcel and environmental (grid-mean) properties within the cloud layer. A moisture factor, which represents the dependence of the entrainment rate on environmental humidity (relative humidity), is combined with the parcel state-dependent entrainment rate model of Gregory (2001). Entrainment rate modeling is shown to be crucial for the sensitivity of cloud top to environmental moisture. To determine the detrainment rate, we assumed a linear decrease of the updraft mass flux to zero at cloud top above the maximum buoyancy level. A hybrid closure method, which blends CAPE and sub-cloud layer vertical velocity scale closures,

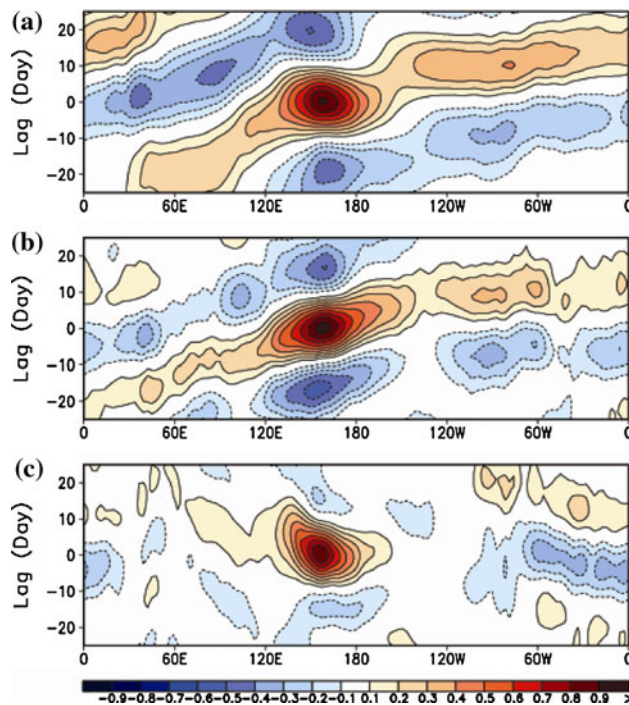


Fig. 16 November–April lag–longitude diagram of 10°S – 10°N averaged intraseasonal U850 anomalies correlated against to the west Pacific reference point (155 – 160°E , 5°S – 5°N averaged). **a** NCEP/NCAR, **b** BMF, and **c** RAS

is used to calculate the base mass flux to account for both cloud layer instability and subcloud layer turbulent kinetic energy as factors in the strength of cumulus. The hybrid

approach for closure is based on the consideration that cumulus cloud is controlled by both the instability within cloud layer and sub-cloud layer turbulent kinetic energy.

The moisture sensitivity of the convection scheme developed is examined in a single time step experiment, by specifying composited temperature and humidity profiles from observation data as an initial condition. The composite is based on PW, inspired by a recent observational study (Holloway and Neelin 2009). It is shown in a single time step experiment that the BMF convection scheme produces the sensitivity of convection to environmental humidity in a similar way to that observed. The updraft mass flux simulated by BMF has a higher top and a stronger magnitude when column is more humid. The sensitivity of convection to environmental moisture is not adequately represented in RAS. The dependence of entrainment rate on environmental humidity, as well as parcel buoyancy and vertical velocity is shown to be important to simulate moisture sensitivity of convection. The hybrid closure method also helps to represent proper moisture sensitivity of strength of convection.

The convection scheme developed is evaluated in the single column framework by specifying observed horizontal and vertical advections of temperature and specific humidity as a forcing to the SCM. The selected periods include the suppressed and active convection regimes and the transition between them. SCM results with two different convection schemes are compared with observed and CRM simulated variables. RAS shows a dry (wet) bias in the lower (upper) troposphere, similar to the bias of AGCM. By comparing mass flux and relative humidity, it is shown that BMF provides a better simulation of the updraft mass flux and relative humidity compared to RAS. When implemented in AGCM, BMF is able to simulate reasonable time-mean precipitation pattern, although it shows wet bias over the northwest Pacific and the SPCZ regions without air-sea interaction. Also, the representation of eastward propagating intraseasonal variability in the tropics is improved in BMF compared to RAS, with enhanced coupling of convection to environmental humidity condition.

Our results suggest that the observed relationship between convection and environmental moisture can be better simulated by improving a conventional convection scheme without using CRMs in each grid of the model. One of the most important factors to achieve this is fractional entrainment rate parameterization, which is a poorly understood process currently. The relationship is thought to be crucial for better simulation of various climate phenomena, such as the diurnal cycle and CCEW, based on previous observational and modeling studies. The impact

of the new bulk mass flux convection scheme on climate simulation will be examined in the further work.

References

- Arakawa A, Schubert WH (1974) Interaction of a cumulus cloud ensemble with the large-scale environment, part I. *Journal of the Atmospheric Sciences* 31:674–701
- Bechtold P, Köhler M, Jung T, Doblas-Reyes F, Leutbecher M, Rodwell MJ, Vitart F, Balsamo G (2008) Advances in simulating atmospheric variability with the ECMWF model: From synoptic to decadal time-scales. *Q J R Meteorol Soc* 134:1337–1351. doi:10.1002/qj.289
- Biasutti M, Sobel AH, Kushnir Y (2006) AGCM precipitation biases in the tropical Atlantic. *J Clim* 19:935–958
- Bonan GB (1996) A land surface model (LSM version 1.0) for ecological, hydrological, and atmospheric studies: technical description and user's guide. PB-97-131494/XAB, National Center for Atmospheric Research, Boulder, CO (United States) (Climate and Global Dynamics Div)
- Bretherton CS, Smolarkiewicz PK (1989) Gravity waves, compensating subsidence and detrainment around cumulus clouds. *Journal of the Atmospheric Sciences* 46:740–759
- Bretherton CS, Peters ME, Back LE (2004) Relationships between water vapor path and precipitation over the tropical oceans. *J Clim* 17:1517–1528
- Brown RG, Zhang C (1997) Variability of midtropospheric moisture and its effect on cloud-top height distribution during TOGA COARE*. *Journal of the Atmospheric Sciences* 54:2760–2774
- Chaboureaud J-P, Guichard F, Redelsperger J-L, Lafore J-P (2004) The role of stability and moisture in the diurnal cycle of convection over land. *Q J R Meteorol Soc* 130:3105–3117. doi:10.1256/qj.03.132
- Chou MD, Suarez MJ (1994) An efficient thermal infrared radiation parameterization for use in general circulation models. NASA Tech Memo 104606:85
- Chou MD, Suarez MJ (1999) A solar radiation parameterization for atmospheric studies. Technical report series on global modeling and data assimilation, NASA Tech Memo 15:40
- Ciesielski PE, Johnson RH, Haertel PT, Wang J (2003) Corrected TOGA COARE sounding humidity data: impact on diagnosed properties of convection and climate over the warm pool. *J Clim* 16:2370–2384
- Cohen C (2000) A quantitative investigation of entrainment and detrainment in numerically simulated cumulonimbus clouds. *Journal of the Atmospheric Sciences* 57:1657–1674
- de Roode SR, Duynkerke PG, Siebesma AP (2000) Analogies between massflux and Reynolds-averaged equations. *J Atmos Sci* 57:1585–1598
- De Rooy WC, Siebesma AP (2008) A simple parameterization for detrainment in shallow cumulus. *Mon Weather Rev* 136:560–576
- Derbyshire SH, Beau I, Bechtold P, Grandpeix JY, Piriou JM, Redelsperger JL, Soares PMM (2004) Sensitivity of moist convection to environmental humidity. *Quarterly Journal of the Royal Meteorological Society* 130:3055–3079
- Grabowski WW (2003) MJO-like coherent structures: Sensitivity simulations using the cloud-resolving convection parameterization (CRCP). *Journal of the Atmospheric Sciences* 60:847–864
- Grant ALM (2001) Cloud-base fluxes in the cumulus-capped boundary layer. *Q J R Meteorol Soc* 127:407–421. doi:10.1002/qj.49712757209

- Grant ALM, Brown AR (1999) A similarity hypothesis for shallow-cumulus transports. *Q J R Meteorol Soc* 125:1913–1936. doi: [10.1002/qj.49712555802](https://doi.org/10.1002/qj.49712555802)
- Gregory D (2001) Estimation of entrainment rate in simple models of convective clouds. *Q J R Meteorol Soc* 127:53–72. doi: [10.1002/qj.49712757104](https://doi.org/10.1002/qj.49712757104)
- Holloway CE, Neelin JD (2009) Moisture vertical structure, column water vapor, and tropical deep convection. *Journal of the Atmospheric Sciences* 66:1665–1683
- Holtlag AAM, Boville BA (1993) Local versus nonlocal boundary-layer diffusion in a global climate model. *J Clim* 6:1825–1842
- Holtlag AAM, Moeng CH (1991) Eddy diffusivity and countergradient transport in the convective atmospheric boundary layer. *Journal of the Atmospheric Sciences* 48:1690–1698
- Huffman GJ, Adler RF, Morrissey MM, Bolvin DT, Curtis S, Joyce R, McGavock B, Susskind J (2001) Global precipitation at one-degree daily resolution from multisatellite observations. *Journal of Hydrometeorology* 2:36–50
- Jakob C, Siebesma AP (2003) A new subcloud model for mass-flux convection schemes: Influence on triggering, updraft properties, and model climate. *Mon Weather Rev* 131:2765–2778
- Johnson DE, Tao WK, Simpson J, Sui CH (2002) A study of the response of deep tropical clouds to large-scale thermodynamic forcings. Part I: modeling strategies and simulations of TOGA COARE convective systems. *Journal of the Atmospheric Sciences* 59:3492–3518
- Kalnay E, Kanamitsu M, Kistler R, Collins W, Deaven D, Gandin L, Iredell M, Saha S, White G, Woollen J, Zhu Y, Chelliah M, Ebisuzaki W, Higgins W, Janowiak J, Mo KC, Ropelewski C, Wang J, Leetmaa A, Reynolds R, Jenne R, Joseph D (1996) The NCEP/NCAR 40-year reanalysis project. *Bull Am Meteorol Soc* 77:437–471
- Khairoutdinov M, Randall DA (2001) A cloud resolving model as a cloud parameterization in the NCAR community climate system model: preliminary results. *Geophys Res Lett* 28:3617–3620
- Kim D, Kug JS, Kang IS, Jin FF, Wittenberg AT (2008) Tropical Pacific impacts of convective momentum transport in the SNU coupled GCM. *Climate Dynamics* 31:213–226
- Klemp JB, Wilhelmson RB (1978) The simulation of three-dimensional convective storm dynamics. *Journal of the Atmospheric Sciences* 35:1070–1096
- Kuang Z, Bretherton CS (2006) A mass-flux scheme view of a high-resolution simulation of a transition from shallow to deep cumulus convection. *Journal of the Atmospheric Sciences* 63:1895–1909
- Le Treut H, Li ZX (1991) Sensitivity of an atmospheric general circulation model to prescribed SST changes: Feedback effects associated with the simulation of cloud optical properties. *Climate Dynamics* 5:175–187
- Lee MI, Kang IS, Kim JK, Mapes BE (2001) Influence of cloud-radiation interaction on simulating tropical intraseasonal oscillation with an atmospheric general circulation model. *Journal of Geophysical Research-Atmospheres* 106:14219–14233
- Lee MI, Kang IS, Mapes BE (2003) Impacts of cumulus convection parameterization on aqua-planet AGCM simulations of tropical intraseasonal variability. *J Meteorol Soc Jpn* 81:963–992
- Lee MI, Schubert SD, Suarez MJ, Schemm JKE, Pan HL, Han J, Yoo SH (2008) Role of convection triggers in the simulation of the diurnal cycle of precipitation over the United States Great Plains in a general circulation model. *Journal of Geophysical Research-Atmospheres* 113:D02111
- Lin C (1999) Some bulk properties of cumulus ensembles simulated by a cloud-resolving model. Part II: Entrainment profiles. *Journal of the Atmospheric Sciences* 56:3736–3748
- Lin YL, Farley RD, Orville HD (1983) Bulk parameterization of the snow field in a cloud model. *J Appl Meteorol* 22:1065–1092
- Lin JL, Kiladis GN, Mapes BE, Weickmann KM, Sperber KR, Lin WY, Wheeler M, Schubert SD, Del Genio A, Donner LJ, Emori S, Gueremy J-F, Hourdin F, Rasch PJ, Roeckner E, Scinocca JF (2006) Tropical intraseasonal variability in 14 IPCC AR4 climate models. Part I: Convective signals. *J Clim* 19:2665–2690
- Lin JL, Lee MI, Kim D, Kang IS, Frierson DMW (2008) The impacts of convective parameterization and moisture triggering on AGCM-simulated convectively coupled equatorial waves. *J Clim* 21:883–909
- Maloney ED, Hartmann DL (2001) The sensitivity of intraseasonal variability in the NCAR CCM3 to changes in convective parameterization. *J Clim* 14:2015–2034
- Moncrieff MW, Krueger SK, Gregory D, Redelsperger JL, Tao WK (1997) GEWEX cloud system study (GCSS) working group 4: precipitating convective cloud systems. *Bull Am Meteorol Soc* 78:831–845
- Moorthi S, Suarez MJ (1992) Relaxed Arakawa-Schubert. A parameterization of moist convection for general circulation models. *Mon Weather Rev* 120:978–1002
- Nakajima T, Tsukamoto M, Tsushima Y, Numaguti A, Kimura T (1995) Modelling of the radiative process in a AGCM. *Clim Syst Dyn Modell* 3:104–123
- Neale RB, Richter JH, Jochum M (2008) The impact of convection on ENSO: from a delayed oscillator to a series of events. *J Clim* 21:5904–5924
- Neggers RAJ, Siebesma AP, Lenderink G, Holtlag AAM (2004) An evaluation of mass flux closures for diurnal cycles of shallow cumulus. *Mon Weather Rev* 132:2525–2538
- Nordeng TE (1994) Extended versions of the convective parameterization scheme at ECMWF and their impact on the mean and transient activity of the model in the tropics. *European Centre for Medium-Range Weather Forecasts*
- Numaguti A, Takahashi M, Nakajima T, Sumi A (1995) Development of an atmospheric general circulation model. *Climate System Dynamics and Modeling* 3:1–27
- Ogura Y, Cho HR (1973) Diagnostic determination of cumulus cloud populations from observed large-scale variables. *Journal of the Atmospheric Sciences* 30:1276–1286
- Petch JC, Willett M, Wong RY, Woolnough SJ (2007) Modelling suppressed and active convection. Comparing a numerical weather prediction, cloud-resolving and single-column model. *Q J R Meteorol Soc* 133:1087–1100. doi: [10.1002/qj.109](https://doi.org/10.1002/qj.109)
- Randall DA, Curry J, Duynkerke P, Krueger S, Miller M, Moncrieff M, Ryan B, Starr D, Rossow W, Tselioudis G, Wielicki B (2000) The second GEWEX cloud system study science and implementation plan. *IGPO Publication Series* 34:45
- Raymond DJ (2001) A new model of the Madden-Julian oscillation. *J Atmos Sci* 58:2807–2819
- Ridout JA (2002) Sensitivity of tropical Pacific convection to dry layers at mid-to upper levels: simulation and parameterization tests. *Journal of the Atmospheric Sciences* 59:3362–3381
- Rutledge SA, Hobbs PV (1984) The mesoscale and microscale structure and organization of clouds and precipitation in midlatitude cyclones. XII: A diagnostic modeling study of precipitation development in narrow cold-frontal rainbands. *Journal of the Atmospheric Sciences* 41:2949–2972
- Sherwood SC (1999) Convective precursors and predictability in the tropical western pacific. *Mon Weather Rev* 127:2977–2991
- Sherwood SC, Minnis P, McGill, M (2004) Deep convective cloud-top heights and their thermodynamic control during CRYSTAL-FACE. *J Geophys Res* 109:D20119. doi: [10.1029/2004JD004811](https://doi.org/10.1029/2004JD004811)
- Siebesma AP (1998) Shallow cumulus convection. *Buoyant Convection in Geophysical Flows* 513:441–486
- Simpson J, Wiggert V (1969) Models of precipitating cumulus towers. *Mon Weather Rev* 97:471–489
- Stan C, Khairoutdinov M, DeMott CA, Krishnamurthy V, Straus DM, Randall DA, Kinter III JL, Shukla J (2010) An ocean–

- atmosphere climate simulation with an embedded cloud resolving model. *Geophys Res Lett* 37:L01702. doi:[10.1029/2009GL040822](https://doi.org/10.1029/2009GL040822)
- Swann H (2001) Evaluation of the mass-flux approach to parameterizing deep convection. *Q J R Meteorol Soc* 127:1239–1260. doi:[10.1002/qj.49712757406](https://doi.org/10.1002/qj.49712757406)
- Takayabu YN, Yokomori J, Yoneyama K (2006) A diagnostic study on interactions between atmospheric thermodynamic structure and cumulus convection over the tropical western Pacific Ocean and over the Indochina Peninsula. *象集誌* 84:151–169
- Tao WK, Simpson J (1993) Goddard cumulus ensemble model. Part I: Model description. *Terr Atmos Oceanic Sci* 4:35–72
- Tao WK, Simpson J, Baker D, Braun S, Chou MD, Ferrier B, Johnson D, Khain A, Lang S, Lynn B (2003) Microphysics, radiation and surface processes in the Goddard Cumulus Ensemble (GCE) model. *Meteorology and Atmospheric Physics* 82:97–137
- Thayer-Calder K, Randall DA (2009) The role of convective moistening in the Madden-Julian oscillation. *J Atmos Sci* 66:3297–3312
- Tiedtke M (1984) The sensitivity of the time-mean large-scale flow to cumulus convection in the ECMWF model. 297–316
- Tiedtke M (1989) A comprehensive mass flux scheme for cumulus parameterization in large-scale models. *Mon Weather Rev* 117:1779–1800
- Tokioka T, Yamazaki K, Kitoh A, Ose T (1988) The equatorial 30–60 day oscillation and the Arakawa-Schubert penetrative cumulus parameterization. *J Meteorol Soc Jpn* 66:883–901
- Tompkins AM (2001) Organization of tropical convection in low vertical wind shears: the role of water vapor. *Journal of the Atmospheric Sciences* 58:529–545
- Troen IB, Mahrt L (1986) A simple model of the atmospheric boundary layer; sensitivity to surface evaporation. *Boundary-Layer Meteorology* 37:129–148
- Uppala SM et al (2005) The ERA-40 re-analysis. *Quart J Roy Meteor Soc* 131:2961–3012
- Wang WQ, Schlesinger ME (1999) The dependence on convection parameterization of the tropical intraseasonal oscillation simulated by the UIUC 11-layer atmospheric GCM. *J Clim* 12:1423–1457
- Wang B, Ding Q, Fu X, Kang I-S, Jin K, Shukla J, Doblus-Reyes F (2005) Fundamental challenge in simulation and prediction of summer monsoon rainfall. *Geophys Res Lett* 32:L15711. doi:[10.1029/2005GL022734](https://doi.org/10.1029/2005GL022734)
- Webster PJ, Lukas R (1992) TOGA COARE: The coupled ocean-atmosphere response experiment. *Bull Am Meteorol Soc* 73:1377–1416
- Willett MR, Bechtold P, Williamson DL, Petch JC, Milton SF, Woolnough SJ (2008) Modelling suppressed and active convection: comparisons between three global atmospheric models. *Q J R Meteorol Soc* 134:1881–1896. doi:[10.1002/qj.317](https://doi.org/10.1002/qj.317)
- Wu XQ, Liang XZ, Zhang GJ (2003) Seasonal migration of ITCZ precipitation across the equator: why can't GCMs simulate it? *Geophys Res Lett* 30:1824
- Wu R, Kirtman B, Pegion K (2006) Local air-sea relationship in observations and model simulations. *J Climate* 19:4914–4932
- Wu X, Deng L, Song X, Vettoretti G, Peltier WR, Zhang GJ (2007) Impact of a modified convective scheme on the Madden-Julian oscillation and El Niño-Southern oscillation in a coupled climate model. *Geophys Res Lett* 34:16823